Journal of Hydrology 644 (2024) 131999

Contents lists available at ScienceDirect

Journal of Hydrology

journal homepage: www.elsevier.com/locate/jhydrol

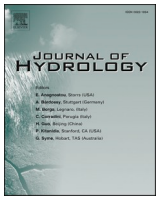

Research papers

Nubian aquifer linkage to the High Aswan Dam Reservoir: Initial assessments of processes and challenges

Mohamed Ramah [a,b], Essam Heggy [c,d,*], Ahmed Nasr [e], Mostafa Toni [f,g], Mohamed M. Gomaa [b], Emmanuel Hanert [a,h], Adel Kotb [f]

[a] Earth and Life Institute (ELI), Université catholique de Louvain (UCLouvain), Louvain-la-Neuve, Belgium
[b] Geophysical Sciences Department, National Research Centre, Cairo, Egypt
[c] University of Southern California, Viterbi School of Engineering, Los Angeles, CA 90089, USA
[d] Jet Propulsion Laboratory, California Institute of Technology, 4800 Oak Grove Drive, Pasadena, CA, USA
[e] Geophysics Department, Desert Research Center, Cairo, Egypt
[f] Geology Department, Faculty of Science, Helwan University, Cairo, Egypt
[g] National Program for Earthquakes and Volcanoes, Geohazard Center, Saudi Geological Survey (SGS), Jeddah, Saudi Arabia
[h] Institute of Mechanics, Materials and Civil Engineering (IMMC), Université catholique de Louvain (UCLouvain), Louvain-la-Neuve, Belgium

ARTICLE INFO

This manuscript was handled by Huaming Guo, Editor-in-Chief

Keywords:
Surface water-groundwater exchanges
High Aswan Dam
Time-domain electromagnetic method
Aeromagnetic survey
Vertical electrical resistivity sounding and water stress

ABSTRACT

Egypt, relying heavily on the Nile as its primary water resource, is facing a rising water budget deficit due to increasing consumption, hydroclimatic changes, and upstream river damming. To address the above, innovative management of High Aswan Dam Reservoir (HADR), the third largest artificial reservoir on Earth, and its exchange with the surrounding groundwater system is suggested to develop new agricultural areas. However, the interconnectivity mechanism between the HADR and the fossil Nubian aquifer, the largest transboundary aquifer in Africa, remains speculative due to the lack of in-situ investigations. To address this deficiency, we perform a geophysical survey using aeromagnetic, time-domain electromagnetic, and vertical electrical resistivity sounding in a 330 km^2 pilot area to the northwest of the HADR that is hypothesized to have a dense fracture system that could act as a conduit between these two large water bodies. Our survey results show the presence of normal faults cross the reservoir to the tangential basement and the sedimentary cover that are water-saturated and act as recharges to the Nubian fossil aquifer. These in-situ investigations confirm previous orbital gravity observations by GRACE-FO hypothesizing the interconnectivity between the reservoir and the Nubian aquifer, which was subject to debate. We suggest that such connecting areas between these two water bodies can be optimal sites for future agricultural development using improved management of surface water-groundwater exchanges for irrigation. Finally, our findings highlight upcoming challenges for this linkage if the level of HADR reaches below ~160 m above mean sea level (amsl) due to upstream dam operation during the Nile's extended drought periods. Under these conditions, the Nubian aquifer could discharge back into the HADR at the investigated site, changing the water budget of the aquifer and compromising the planned agriculture developments in the adjacent areas, which account for ~ 10 % of the total arable land in Egypt.

1. Introduction

Egypt is Africa's most populous, arid, and water-scarce country, with a water share per capita of ~560 m^3 (Fouad et al., 2023), classifying it as severe water stress. The implications of this alarming and rising water scarcity on food security and the national and regional socioeconomic stabilities are major, including social unrest and outflow migration (Heggy et al., 2023, 2022a, 2021). As such, the nation seeks to achieve a sustainable water management strategy by 2030 to address the above threats. Egypt primarily relies on surface water resources from the Nile to irrigate its agricultural land, mainly located on the banks of the river and in its Delta (Abotalib et al., 2023). These arable lands represent 4 % of the country's total area, while the other 96 % are arid deserts (Fouad et al., 2022, 2023; Nikiel and Eltahir, 2021). These planted areas are home to ~95 % of its inhabitants (FAO, 2016). During the last decades, all of the water requirements for developmental activities in Egypt were

* Corresponding author.
E-mail address: heggy@usc.edu (E. Heggy).

https://doi.org/10.1016/j.jhydrol.2024.131999

Available online 18 September 2024

fulfilled by the Nile (Heggy et al., 2022b). However, population growth and the rising demand for water usage and food production, as well as the increase in the size of urban areas to the detriment of the agricultural land and the increase in upstream damming, has resulted in a large water budget deficit beyond the average yearly flow (Heggy et al., 2022a; Yousif, 2019). For instance, the Grand Ethiopian Renaissance Dam (GERD) operation is projected to alter the High Aswan Dam Reservoir (HADR) during extended drought periods. GERD reservoir can adjust the flow of the Nile River, which could reduce the stored water budget downstream in the reservoir (Heggy et al., 2023). A decrease in the flow of the Nile due to GERD operations could lead to lower water levels in HADR, reducing the amount of water available for recharge into the Nubian Sandstone Aquifer System (NSAS). Therefore, the Egyptian authorities proposed groundwater resources and HADR management as the main mitigations to address the nation's budget deficit (Fathy et al., 2021). Expanding groundwater extraction and HADR water management is considered one of several proposed mitigations of water scarcity in Egypt (Heggy et al., 2021).

The HADR is considered the nation's largest strategic water reserve, with a maximum volume of 162 Billion Cubic Meters (BCM) (Eldardiry and Hossain, 2021). However, it suffers from high evaporation(Elba et al., 2014) and seepage losses to the adjacent Nubian Sandstone Aquifer (NSSA). While the evaporation is well constrained based on accurate atmospheric observation (Hassan et al., 2018). The modeled seepage recharge and the connectivity between the HADR and NSSA are widely debated and uncertain (Diab, 1972; EI-Difrawy, 1988; Elsawwaf et al., 2014; Ghoubachi and El-Abd, 2016; Kim and Sultan, 2002; Metwaly et al., 2006; Rabe et al., 2009). For instance, the use of the Gravity Recovery and Climate Experiment (GRACE) suggests that during high stands of HADR, the seepage from HADR to NSSA accounts for 6 BCM per year (Abdelmohsen et al., 2020). The evaluation of this volume of seepage as a function of the HADR water content is subject to active research. The potential impacts of this seepage on the surrounding environment of HADR, including changing groundwater levels, soil stability, and the potential for developing new agricultural areas (Hanna and Osman, 1995), is a subject of scientific and public interest. However, with high uncertainties, these studies diverge on the direction of the connection and the amount of seepage from HADR to NSSA. To address the above, we perform a geophysical survey using aeromagnetic, Time Domain Electromagnetic (TEM), and Vertical Electrical Resistivity Sounding (VES) at a 330 km pilot area located Northwest of the HADR (Fig. 1a), which is one of the planned areas (Abdelkhalek and King-Okumu, 2021), for new agriculture development around HADR to increase the national agriculture area. As such, assessing the groundwater resources in this pilot area and their recharge through structural conduits from the High Aswan Dam reservoir is crucial for achieving sustainable agricultural development projects. Understanding the seepage from HADR to the NSSA is crucial in this regard. This can be achieved using the aeromagnetic, electrical resistivity, and electromagnetic methods, which effectively assess groundwater conduits and structure-controlled recharge (Gaber et al., 2020; Gonzales et al., 2016; Kotb et al., 2014; McClymont et al., 2011; Kirsch, 2006).

The three objectives of our geophysical investigation in the pilot study area are, first, the identification of water-bearing formations; second, the determination of the geoelectrical characteristics of the aquifer basement relief; and third, the elicitation of subsurface structures that act as a groundwater conduit between the aquifer and HADR. Based on the above, we provide the optimal locations for drilling boreholes to supply irrigation water for future sustainable agriculture development along the pilot study area.

2. Geological setting

The study area is located northwest of the HADR between 23°40′19.21″N to 23°46′14.42″N and 32°33′45.20″E to 32°47′31.74″E and covers an area of about ~ 330 km^2 (Fig. 1a). This area represents the Nubian plain of the eastern part of the sandstone Pedi plain (Said, 1975) and extends from the boundaries of the HADR in the east to Gilf El-Kebir in the west. It is composed mainly of Nubian sandstone (Abou Elmagd et al., 2014; Embabi, 2004; El-Naggar, 1970) with elevation ranging from 100-200 m above mean sea level (amsl) (Fig. 1b). The Nubian sandstone in the study area consists of Abu-Aggag and Timsah formations. The former belongs to the Turonian age and consists of conglomerate sandstone with coarse-grained kaolinite overlying unconformable basement rocks (Issawi, 1978; CONCO, 1987; Issawi, 1973), while the latter is composed of near-shore marine to deltaic sequences of shale, silt, and sandstone with oolitic iron ore beds (Fig. 1c; CONCO, 1987). Structurally, the West Aswan area is affected by two fault systems (Fig. 1c) with trends almost in the N–S and E–W directions (Araffa et al., 2018; Idriss et al., 1985; Issawi, 1978; Mekkawi et al., 1982). Some of these faults are strike slips (Awad and Kwiatek, 2005; Fat-Helbary and Tealb, 2002; Mekkawi et al., 2005). Hydrogeologically, the Abu-Aggag sandstone represents the main water-bearing formation in the west Aswan area. The water-bearing layers are separated by semi-confining clay intercalations (Geoistrazivanja Hamdan et al., 2013; Selim, 1986; Shedid, 2006). This water-bearing layer has not yet been thoroughly detailed in different places (Yousif, 2019), which we address in the present study.

3. Datasets and processing

Integrating multiple geophysical datasets, including aeromagnetic, TEM, and electrical resistivity data, can provide complementary information (Basheer et al., 2024; Gomaa et al., 2024; Kotb et al., 2021; Ebraheem et al., 2016) that reduces uncertainty in hydrogeological models. By constraining model parameters with geophysical observations, such as aquifer geometry, hydraulic properties, and boundary conditions, it becomes possible to improve the groundwater flow simulation accuracy and prediction accuracy (Basheer et al., 2024). In the present study, we used three geophysical investigation methods to assess the potential presence of groundwater conduits between the reservoir and the Nubian aquifer: Aeromagnetic, TEM, and VES.

Aeromagnetic data are used to identify geological structures such as faults, fractures, and lithological variations that may influence groundwater flow and storage, such as regions with shallow aquifers or areas of concentrated faulting and fracturing (Kivior and Boyd, 1998; Ramah, 2021). TEM surveys provide information about subsurface resistivity contrasts, which can help delineate aquifer boundaries and preferential flow pathways of the NSSA from HADR over the pilot study area (Mosaad et al., 2024). Integrating these datasets allows for a more comprehensive understanding of the spatial distribution of groundwater-bearing formations and connectivity (Kotb et al., 2014). Electrical resistivity surveys are used to estimate parameters such as hydraulic conductivity, porosity, and water content within aquifer formations. By combining resistivity data with TEM surveys, which offer depth penetration capabilities, it becomes possible to infer variations in subsurface lithology, water saturation, and aquifer properties over a range of depths (Sultan and Santos, 2009). This integrated approach enhances the characterization of hydrogeological properties and improves groundwater resource assessment (Kotb et al., 2021; Sultan and Santos, 2009). Accordingly, the electrical method is used as a supportive method to the TEM survey at shallow depth and probes most upper geologic layers in the study area to 150 m.

We also used geological exposures, hand-dug, and drilled water wells (Fig. 2) to collect all available hydrogeological information to support the interpretation of our geophysical survey.

3.1. Aeromagnetic data

The processed total intensity magnetic map of the study area was obtained from the Egyptian Geological Survey and Mining Authority (EGSMA, 1981). The total magnetic intensity data were extracted from a

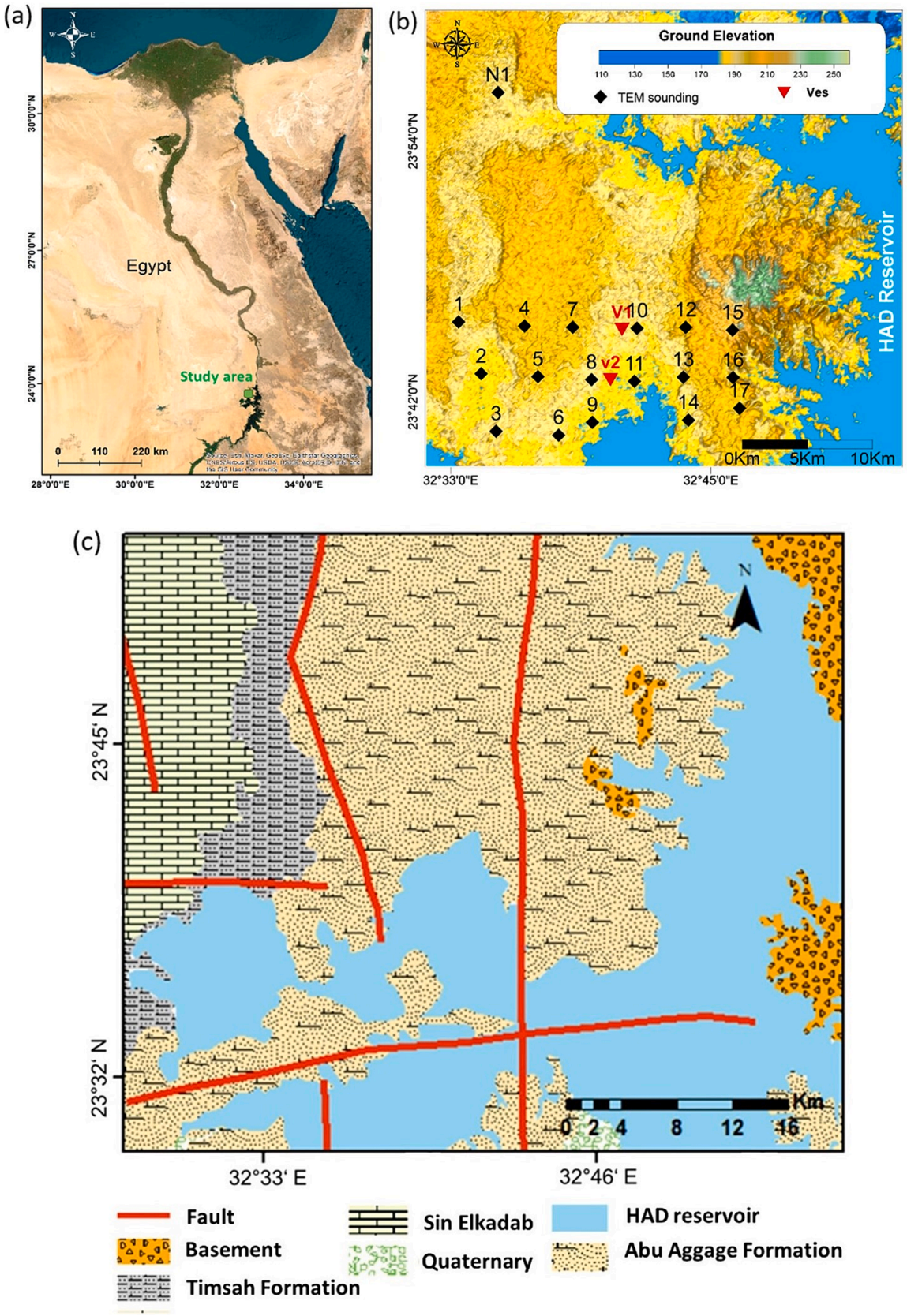

Fig. 1. (a) Satellite image of Egypt showing location of the study area, (b) digital elevation model (DEM) of the study area with spatial location of measured stations, (c) geological map of the study area (modified after CONCO, 1987; Azeem et al., 2014).

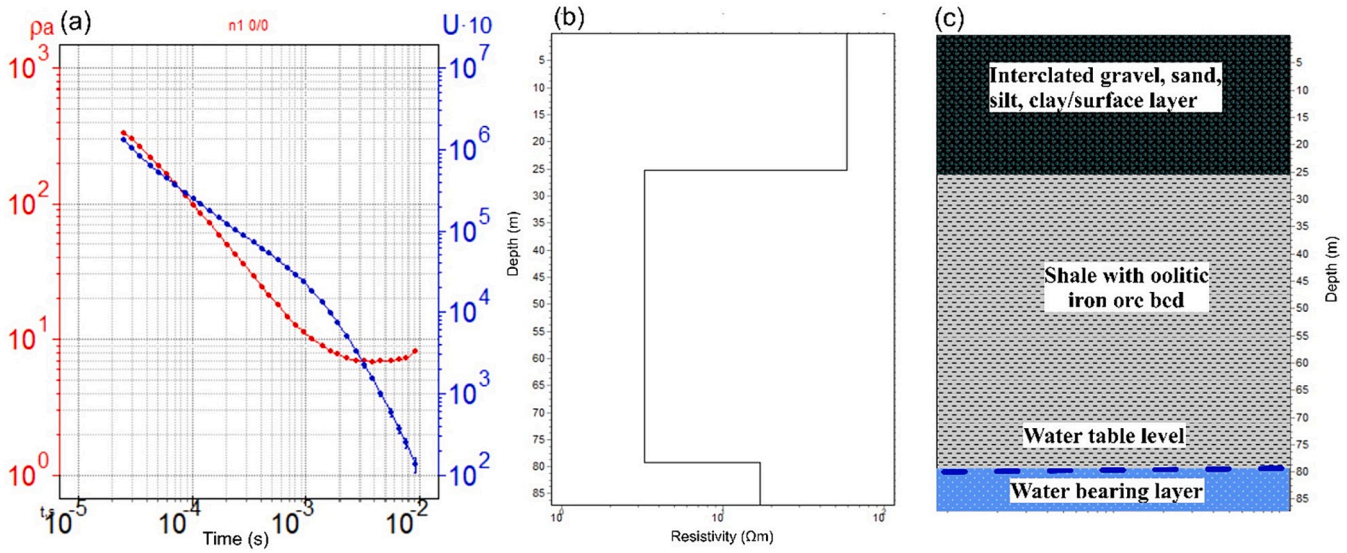

Fig. 2. (a) Measured TEM sounding N1, (b) modeled layers, and (c) lithology records from drilled well near the study area.

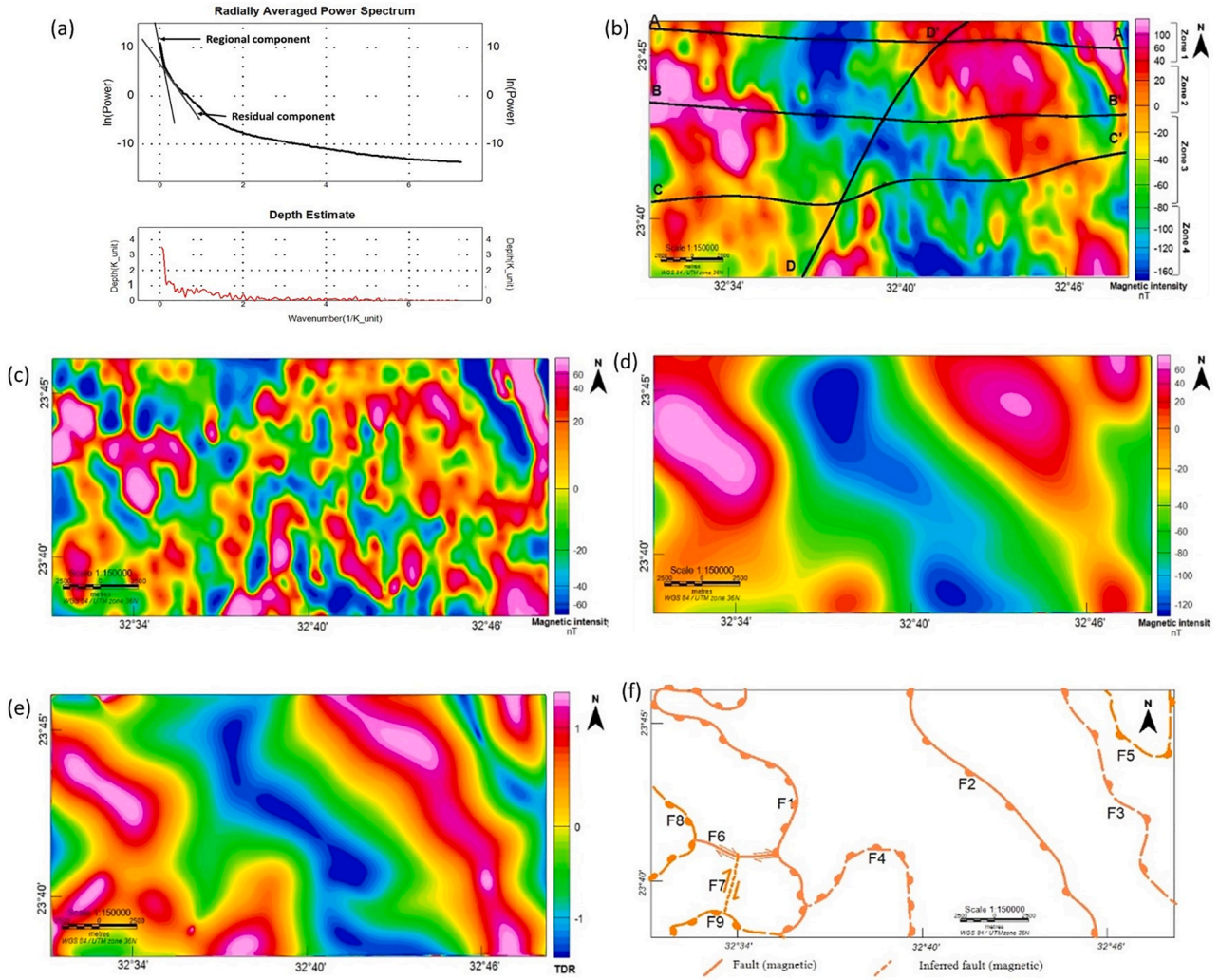

Fig. 3. (a) 2-D radially averaged power spectrum of the RTP magnetic data. (b) RTP map of the study area that is classified into magnetic zones. (c) Gaussian residual filtered (frequency = 0.12–0.4 Cycles/Grid Unit) of residual magnetic map of the study area. (d) Gaussian regional filtered (frequency = 0–0.12 Cycles/Grid Unit) of the regional magnetic map of the study area. (e) Tilt derivative filter (TDR) of the regional map. (f) Regional structure map from TDR Filter.

10 km × 30 km grid. Total magnetic intensity measurements are derived from a 10 km × 30 km grid. The magnetic data are reduced to the magnetic pole to avoid distortion of the shapes, sizes, and locations of magnetic anomalies caused by the inclination of the Earth's magnetic field. The values of the magnetic field for our study area (inclination 32.8 and declination 1.9) are utilized to generate a reduced-to-pole (RTP) magnetic map (Fig. 3b). We applied frequency analysis and filters to the obtained data in the frequency domain utilizing the Fast Fourier Transform (FFT) algorithm of the Oasis Montaj Package (Geosoft Inc, 2010; Fig. 3c, d, e). In addition, we applied a power spectral analysis to determine the regional and residual components of the magnetic anomaly (Fig. 3a, c, d). A Tilt Derivative (TDR) filter is then applied to

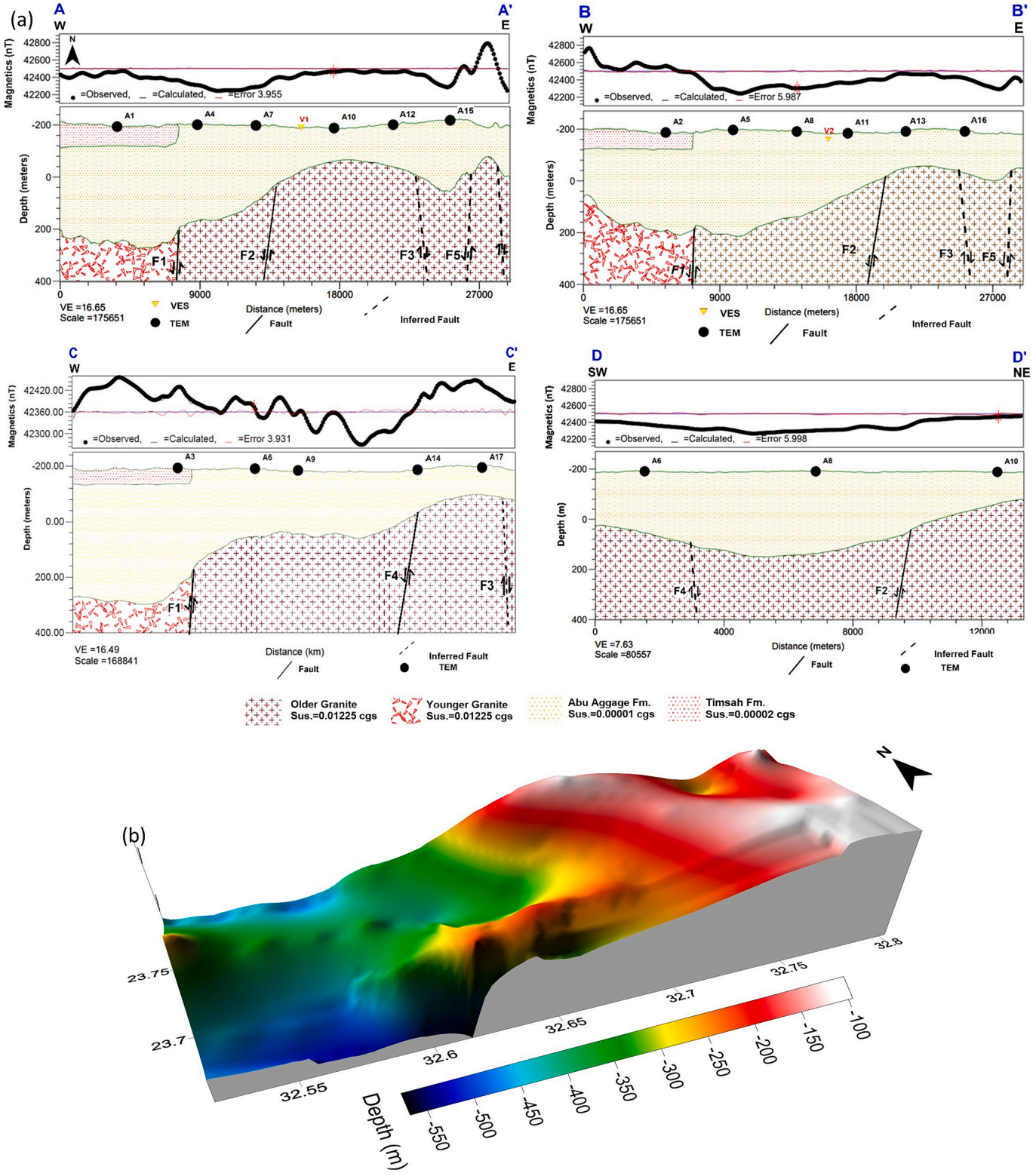

Fig. 4. (a) Interpreted geologic cross sections along the A-A', B-B', C-C' and D–D' profiles (see Fig. 3b for the locations of the selected profiles). (b): 3D depth to basement map of the study area.

the magnetic data to map shallow basement structures (Fig. 3e, f). Also, four 2D magnetic profiles were constructed using 2D modeling techniques using Gm-sys software (Fig. 4a) and mapping the depth to the basement over the study area (Fig. 4b).

3.2. TEM and VES measurements

Seventeen TEM measurements are conducted as a grid along the study area, in addition to one for validation carried out close to a drilled well near the study area and under the same hydrogeological conditions (Fig. 1b). A simple coincident loop configuration (Fitterman and Stewart, 1986) has been employed using a TEM-FAST 48 HPC instrument with single square loop configuration (working as EM transmitter and receiver) with (200 m × 200 m) using current intensity ranges from 1 to 4A. The survey was carried out by repeating the measurement two or three times at the same station to assess the variability of the readings. The most suitable signal-to-noise measurement was selected for further processing steps and interpretation. The individual TEM datasets are

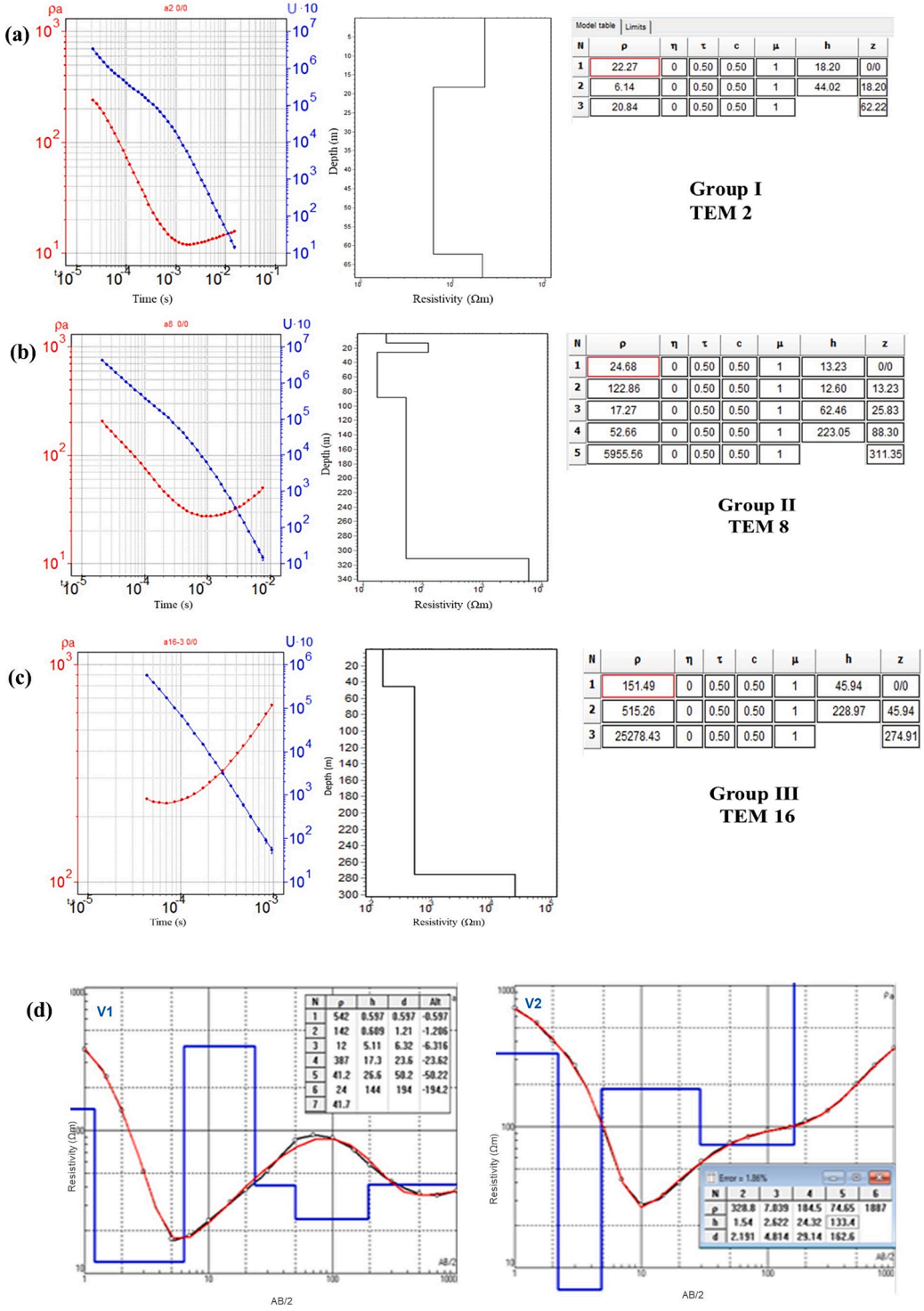

Fig. 5. Examples of interpreted TEM sounding. (a) TEM 1 from geo-electric group I, (b) TEM 8 from geo-electric group II, (c) TEM 16 from geo-electric group III, and (d) VES curves inversion results for V1 and V2.

first iteratively inverted using ZondTEM 1D software (version 5.2).

The VES measurements followed the TEM survey. We used the SYSCAL JUNIOR equipment employed for the sounding. Because of the high resistivity of the surface, the dry Nubian sandstone layer makes transmitting the current into the ground challenging. Several attempts were made to overcome this problem by increasing the number of electrodes used to make a bridge. We also added water near the electrodes to improve connectivity to the ground. However, only two vertical electrical soundings were successfully conducted using the symmetrical Schlumberger electrode spread technique at each of the selected points. The IPI2win Software (Version 3.0.1 s) has been used for resistivity data processing.

The first step in interpreting the sounding results is solving the inverse problem. Basically, based on an initial model, inversion of 1D TEM and VES data is the process of predicting XYZ distribution of layers with different resistivity values. The initial model parameters were integrally constructed from surface general geology and subsurface geological information derived from well N1 (Fig. 2). Examples of the inversion results of three TEM soundings and two VES are depicted in Fig. 5. It has to be noted that the root mean square (RMS) between the observed and the calculated parameters is less than 10 % for all TEM and VES soundings in the study area.

4. Results

Our results of integrating aeromagnetic maps with TEM and electrical resistivity surveys aim at mapping the structural elements of the investigated area, including faults, fractures, and lithological variations, providing insights into groundwater flow between HADR and adjacent Nubian aquifer and identifying preferential conduits and recharge zones, supporting better management of surface water-groundwater exchanges to irrigate new agricultural developments:

4.1. Aeromagnetic results

The examination of the RTP map (Fig. 3b) shows that the investigated area is represented by sets of shallow negative and positive magnetic anomalies with varying amplitudes, wavelengths, sizes, and magnitudes. According to the frequencies of magnetic anomalies amplitudes, the RTP map can be qualitatively segmented into four zones of very high, high, low, and very low amplitude (Fig. 3b). The variation of the amplitudes of these magnetic anomalies may reflect changes in the composition and depth of geologic rocks.

4.1.1. Magnetic spectral analysis

Energy spectrum analysis is a technique that quantitatively assesses large and complex magnetic datasets. Spector and Grant (1970) use a depth analysis technique to compute two-dimensional power spectra from gridded magnetic data. The radially averaged power spectrum of the magnetic data was calculated (Fig. 3a), and the best-fit straight lines of the spectra were determined. The magnetic components of shallow and deep sources were represented by the two best-fit segments that were obtained. The slope/4p of that segment indicates the average depth of the magnetic sources corresponding to each segment. The - average depth values for deep and shallow magnetic sources, respectively, are 0.7 km and 0.1 km from the survey level, according to depth computations done on these segments.

4.1.2. Residual magnetic component map

Examining the map of residual magnetic component (Fig. 3c) bears a striking resemblance to the RTP map (Fig. 3b), which would imply that the majority of basement rocks in the study area which are the cause of the magnetization—are either exposed at shallow depths or are cropping out on the surface. A portion of the magnetic anomalies span a significant geographic area. Furthermore, these anomalies have high magnitudes, high to low frequencies, and moderate to high amplitudes, indicating that the magnetic bodies causing the magnetization are extended at depth.

4.1.3. Regional magnetic component map

The procedures for separation are intended to distinguish between more pronounced local anomalies and broader regional variations (Fig. 3d). This map can be categorized as having low zones (negative magnetic anomalies) in the middle and eastern regions, which are covered in varying thicknesses of Nubian sandstone of the Abu Aggage formation. Their amplitudes reach up to −145 nT. Also, positive magnetic anomalies represent the high zones. They covered the western part of the area and may be interpreted as a structurally high formation (i.e., a horst). They are found as a magnetic mass extending in the western part of the study area and may relate to the remnant magnetization of the oolitic iron bed. Their amplitudes reach 97 nT.

4.1.4. Tilt derivative (TDR) filter

The general structure of the region can be obtained from magnetic data. In addition to supporting the interpretation, filtering the magnetic data brings out and highlights trends and anomalies in the data. Mineral exploration targets and shallow basement structures can be mapped with the help of TDR and its total horizontal derivative. The TDR map has the advantage of having its zero-contour line on or near the fault/contact spot. The TDR filter is applied to the magnetic data deduced from the magnetic interpretation results (Fig. 3e) and used to construct the map of the dominant structure elements affecting the study area (Fig. 3f). The inferred faults affecting the basement and cover sedimentary rocks along the study area are represented by a group of normal faults (F1-F5, F8 and F9) having more or less, NE-SW, NW-SE (Fig. 3f) and other strike-slip faults (F6, F7 and F 10) having more or less E- W and NE-SW trends.

4.1.5. 2D magnetic modeling

Four 2D magnetic profiles (Fig. 3b) are modeled. The RTP magnetic values have been traced along these profiles. Basement structural cross-sections are constructed along these profiles to begin modelling using available geologic information, previously performed magnetic depth determinations, and the results of qualitative interpretation of magnetic maps.

The first profile (A-A') lies in the northern part of the study area and is oriented West to East (Fig. 3b). A closer look at this profile indicates an outstanding match between the observed and calculated anomalies, with an error RMS of 3.955 %. (Fig. 4a). This model comprises two blocks that represent various types of basements in terms of composition and form. Furthermore, the model represents the geological existence of basin and horst areas induced by normal faults affecting the basement in depth ranges between 120 and 462 m along the profile.

The second profile (B-B') is located in the center of the study area (Fig. 3b). The direction of this profile is from West to East (Fig. 4a). This model consists of two blocks that show various types and compositions of the basement. Also, the model reflects the presence of basin and horst areas according to the geologic setting of the study area, which can be interpreted as normal faults affecting the basement. The depth to the basement along this profile ranges between 120–389 m.

The third profile (C-C') is located in the southern part of the study area (Fig. 3b). The direction of this profile is from West to East (Fig. 4a). The basement presents a depth range between 105 and 395 m. The model also reflects the existence of basin and horst zones, which are triggered by faults in the basement (Fig. 4a).

The fourth profile (D-D') is a traverse profile that was drawn to cut the upper three profiles (Fig. 3b). The profile direction is from south to north. This profile reveals an excellent match between the observed and calculated anomalies, with a RMS error of 5.9. (Fig. 4a). A homogeneous basement can be seen in this profile. The basement depth varies between 105 and 340 m along the profile, indicating a graben between two normal faults.

Basement depth map is generated by digitizing the depths of the basement profiles. The interpreted depth to the basement map (Fig. 4b) indicates that the basement is deeper in the middle and western parts than the eastern parts, where the basement depth exceeds 450 m. The basement depth in the eastern parts of the study area reaches less than 100 m. According to Fig. 4b, the maximum sedimentary thickness will be found in the western and some middle parts of the study area, while the minimum sedimentary thickness will be found in the eastern portion.

4.2. 1D and 2D models of TEM and electrical resistivity

The resulting parameters under every discrete point describe a subsurface model involving three or four layers (Fig. 5). These layers are geologically correlated to produce six geoelectrical layers. Some of these layers appear and disappear spatially, forming three different subsurface geoelectrical successions with the aerial distribution. The first geoelectrical succession (I) describes the western portion and consists of three layers; the middle layer corresponds to the Timsah Formation, which rests under the surface layer, while the lower one corresponds to the Abu Aggage Formation (Fig. 5a; Table 1). The second geoelectrical succession (II) covers the middle part of the study area and consists of four layers. The correlation between the available geological information and aeromagnetic data suggests that the upper layer represents the surface layer, the second layer corresponds to dry sandstone, the third layer represents the water-bearing layer (Abu Aggage Formation), and the lowermost layer corresponds to the basement granitic rock (Fig. 5b; Table 1). The third geoelectrical succession (III) covers the eastern side of the study area and consists of two geoelectrical layers under the surface; the first layer represents silicified sandstone over basement granitic rock (Fig. 5c). A detailed description of the six encountered layers, consisting of three groups, is given in Table 1.

The resistivities and thicknesses are presented as 2D visualization cross-sections. The cross-sections in Fig. 6 are shown as a function of their equivalent geologic rock formations. The horizontal and vertical extensions of the dissimilar layers in the West-East direction are shown along the A-A', B-B', and C-C' sections. The changes of geoelectrical parameters in the SW – NE direction at the central part of the study area have been shown in the cross-section (D-D') of the transverse. The generated geoelectrical cross-sections visualize obviously the main geologic features that characterize the study area. Moreover, the above explains the structural relationship between the three detected groups of layering succession (i.e., I, II, and III). According to the geological map of the study area, the relative vertical displacements of the correlated formations in the developed geoelectrical cross-sections, represented by four normal faults affecting the study area, have been inferred (F1-F4). Two faults strike in the NE-SW direction (F1 and F2), and the strike of other faults is NW-SE (F3, F4). Some of these faults are responsible for relatively uplifting the older succession in front of the younger sediments (Faults F1 and F3 at the West and East). The other faults formed the basin base on which the Nubian sandstone sediments were deposited.

Table 1
Ranges of resistivities and thicknesses inferred from the survey data interpretation for different layers with their corresponding lithology and geological formations.

Group	Layer	Resistivity ranges (Ω.m)	Thickness ranges (m)	Suggested geological interpretation (Lithology/ Formation)
(I)	A	22–51	17–27	Silt, sand and gravels/ Surface layer
	B	–	–	–
	C	6–9	41–44	Shale with oolitic iron-ore bed /Timsah formation
	D	21–33	320–380	Water bearing sandstone
	E	–	–	–
	F	–	–	–
(II)	A	24–179	10.-18	Silt, sand and gravels/ Surface layer
	B	106–305	8–19	Dry sandstone
	C	–	–	–
	D	22–45	69–333	Water bearing sandstone
	E	–	–	–
	F	1012-7337	–	Basement
(III)	A	90–151	19–46	Silt, sand and gravels/ Surface layer
	B	–	–	–
	C	–	–	–
	D	–	–	–
	E	515–827	151–229	Silicified Nubian Sandstone
	F	4802-25278	–	Basement

4.3. Priority decision map

To evaluate and assess the water-bearing layer, we used the computed geoelectrical properties (resistivity, thickness, and depth) to create three classified contour maps that depict the spatial distribution of the aquifer (Fig. 7). The resistivity distribution (Fig. 7a) of the Abu Aggage water-bearing layer is characterized by values ranging from 21 to 45 Ω.m). The low values (<30 Ω.m) are found in the western part of the area due to the increase of clay content and/or the presence of iron oxides. The thickness (Fig. 7b) increases from 60 m in the East to a maximum thickness of 400 m in the West, indicating a prevailing Nubian sandstone aquifer acting as a long-term water resource. Generally, the Abu Aggage water-bearing layer could be observed at depths ranging from 18 to 72 m below the ground surface (Fig. 7c). It is shallow and semiconfined at the western part of the area where the cap rock is the Timsah Formation to the unconfined character at the central and eastern parts of the study area.

The priority decision map was generated using resistivity, thickness, and depth with an equal weight of 33.333 % and shows three categories to consider when drilling new water wells (Fig. 7d). Decision-makers could use it to decide where to drill water wells in the best locations and extract groundwater for sustainable development projects. Given higher basement relief and the presence of compact sandstone in the eastern portion, in addition to fault directions, the Nubian sandstone water-bearing layer in the study area is likely to be recharged from the South and not from the East (Fig. 8). This result agrees with the expected recharge model conducted by Yousif (2019).

5. Discussion

Our study investigates the groundwater occurrence, distribution and the potential interconnection between HADR and the Nubian aquifer over a pilot area of 330 km^2 using three geophysical methods: Aeromagnetic, TEM, and VES. Our results (Figs. 3- 6) pertain to three main findings that constrain uncertainties regarding the interconnectivity between HADR and the Nubian aquifer, the potentiality of the aquifer for use in sustainable agriculture projects, the role of structural setting in recharging the Nubian aquifer and the indirect role of upstream damming in affecting the water recharge/discharge between HADR and NSAS.

First, our findings suggested that the main aquifer along the study area is represented by the Abu Aggage formation, which is distributed along the study under semi-confining conditions. In the eastern part of the pilot area, the formation is unconfined, while in the western part, it is under confining conditions due to the existence of an aquitard layer of the Timsah formation above the water-bearing layer. In terms of the resistivity distribution of the water-bearing layer, the water quality ranges from fresh, in the eastern part of the water-bearing formation due to lower clay intercalation, to brackish in the western side due to high intercalated clays (Fig. 7a). The water-bearing layer thickness, ranging from 160 m in the east to 400 m in the west (Fig. 7b), is thick enough to provide the needed water volume to sustain planned projects in the pilot area of 330 km^2 which need ~270 million cubic meters per year for

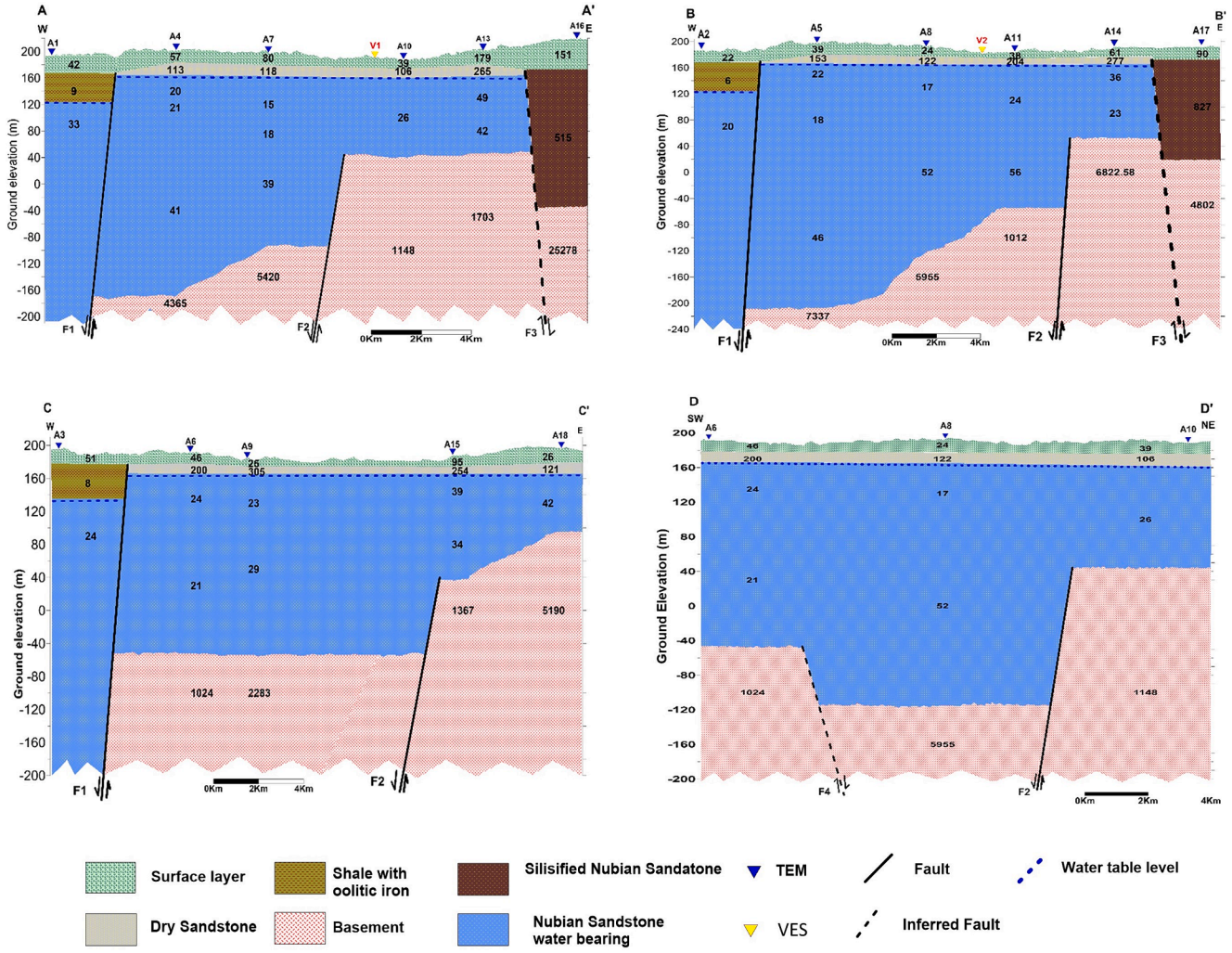

Fig. 6. The four geoelectrical cross-sections inverted from our TEM and VES surveys show the distribution of the geoelectrical layers in relation to their equivalent geologic rock formations. The horizontal and vertical extensions of the dissimilar layers in the West-East direction are shown along the A-A', B-B', and C-C' sections. The changes of geoelectrical parameters in the SW – NE direction in the central part of the study area have been shown in the traverse cross-section (D-D'). The generated geoelectrical cross-sections visualize obviously the main geologic features that characterize the study area. Moreover, they explain the structural relationship between the three detected groups of layering succession (i.e., I, II, and III). The depth of the basement is deduced by the integration of aeromagnetic results (Fig. 4a) and the TEM results.

irrigation. The water-bearing layer along the pilot area is a promising aquifer for use in future sustainable development projects, whether it is industrial, agricultural, or construction of new urban areas. The decision map (Fig. 7d) can support decision-makers in optimizing the implementation of the planned projects in the vicinity of HADR, using the two crucial observations made herein on groundwater quality (as deduced from the water-bearing formation resistivity distribution), groundwater quantity (as deduced from the water-bearing formation thickness) or the borehole drilling depth (deduced from the distribution of the thickness of the water-bearing formation). A separate priority map for each of these observables was constructed (Fig. 7a, b & c). The potentially cultivable area around the HADR is close to one million feddans (420 thousand hectare) (Hanna and Osman, 1995), which can be an increase ranging from 8 to 10 % of the total agricultural area in Egypt.

Second, our findings reveal that the structural setting in the HADR northwestern adjacent area controls the groundwater flow, recharge, and occurrence. Additionally, basement relief plays a crucial role in defining the quantity of the stored groundwater in the pilot site. Depending on their orientation and hydraulic permeability, faults may act as preferential flow paths, directing water toward the aquifer. Conversely, faults can also act as barriers, impeding groundwater movement and impeding recharge patterns. For example, based on our geophysical survey and field observations, in the south-middle part of the studied area, the faults deduced from our survey serve as conduits for surface water infiltration into highly permeable rock formations that allow water to penetrate deeper into the subsurface of the adjacent aquifer (Fig. 8). While in the eastern part, the high basement and associated faults filled by hydrothermal solutions (i.e., quartz veins from field observations) block the direct recharge from HADR to NSAS from the eastern direction resulting in no groundwater existence (Fig. 8).

Third, our findings suggest that the groundwater level in the pilot site ranges from ~160 to 166 m amsl, implying that the recharge from HADR will continue as long as the reservoir level is above ~160 m (Figs. 6, 8). However, if the reservoir level falls below that level, the reverse flow direction from the Nubian aquifer system to HADR can reduce the groundwater level in the adjacent areas to below 160 m. The volume of such reverse discharge requires robust modeling effort to be carried out as a continuity of this investigation in separate work. However, under the prolonged drought period (e.g., 1978–1987 where HADR level falls below 158 m; Abd Ellah, 2020, 2021) or potentially continuous unilateral operation of upstream damming, HADR can be below 160 m for an extended amount of time of a few to multiple years,

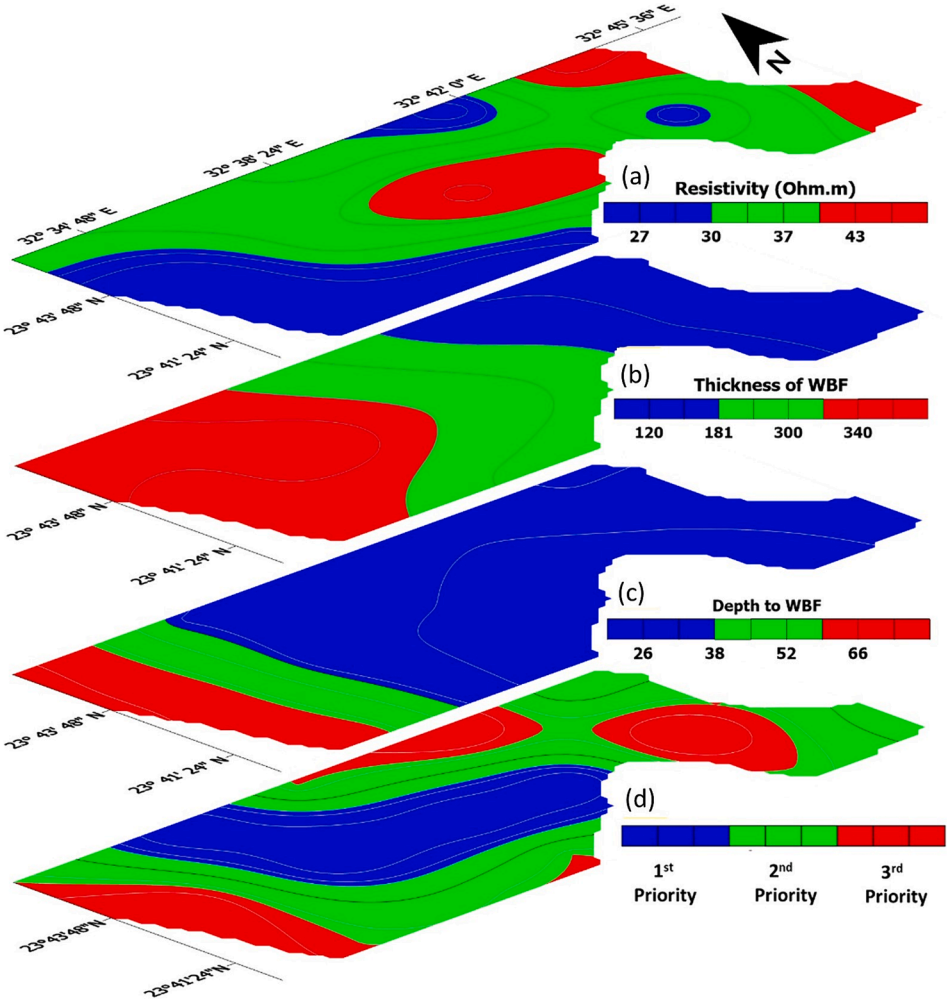

Fig. 7. (a) Iso-resistivity contour map, (b) Isopach map of the water-bearing formation, (c) Depth to water-bearing formation map, and (d) Priority map of the water-bearing formation from the integration of aeromagnetic, TEM, VES results.

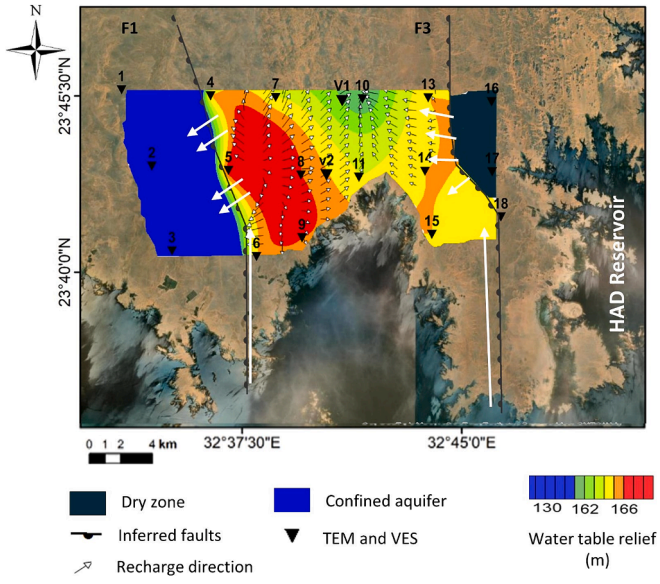

Fig. 8. Direction of the recharge flow in the study area.

increasing the discharge from the NSAS. It is important to note that the average operational water level of HADR within the period of 1965–2020 is 170 m amsl. However, extreme values of 158 m and 182 m amsl were observed at the beginning of 1987 and 1997 (Abd Ellah, 2021). The water levels in HADR exhibit significant seasonal fluctuations, primarily due to the seasonal patterns of the Nile River, which is influenced by the annual rainy season in the Ethiopian Highlands (which feed the Blue Nile). Typically, the levels rise during and after the rainy season (July to October) and fall during the dry season (Elhaddad et al., 2024: Basheer et al., 2024).

GERD has the capacity to regulate the flow of the Blue Nile, which is one of the main tributaries of the Nile River, accounting for 80 % of the river flow (Heggy et al., 2023, 2021). As such, the water released from the GERD can be expected to modulate the level of HADR and, accordingly, the groundwater table depth in its adjacent areas. Under low-release scenarios, this can affect the aquifer sustainability around HADR and then affect the availability of irrigation water and hydropower generation. Hence, alterations in the flow regime of the Nile River due to upstream damming could indirectly influence recharge rates and groundwater levels in the Nubian Aquifer. Proactive management and cooperation among Nile Basin countries is essential for addressing the above potential challenges and ensuring the sustainable management of both surface water and groundwater resources in the Nile Basin.

Finally, quantifying the volume of recharge or discharge from the High Aswan Dam Reservoir to the Nubian Aquifer can be challenging due to several limitations: (1) The hydrogeological system involving the

High Aswan Dam Reservoir, and the Nubian Aquifer is inherently complex, with various interconnected factors influencing water movement and storage. The aquifer heterogeneity, including variations in permeability and porosity, makes it difficult to accurately estimate the volume of water entering or leaving the aquifer. (2) Limited data availability and accessibility, including groundwater levels, aquifer properties, and surface water interactions, can hinder accurate quantification. Insufficient monitoring infrastructure and data collection networks can result in gaps in crucial knowledge for understanding recharge and discharge processes. (3) The interaction between surface water from the Nile River and the Nubian Aquifer further complicates quantification efforts in the absence of in-situ measurement of the hydraulic gradients and flow dynamics. Addressing these limitations requires an interdisciplinary approach combining hydrogeology, hydrology, remote sensing, and modeling techniques that will be conducted as future work.

6. Conclusion and recommendations

In this investigation, we performed a geophysical survey using aeromagnetic, time-domain electromagnetic, and vertical electrical resistivity sounding in a 330 km^2 pilot area northwest of the HADR that is hypothesized to have a dense fracture system that could act as a conduit between these two water bodies. The aquifer connection with HADR has been geophysically confirmed, suggesting an ongoing recharge of the NSAS. Our subsurface mapping suggests that the structural setting plays a major role in groundwater flow and recharge, acting as a conduit between HADR and NSAS. Such connecting areas could be promising sites for sustainable agricultural development projects due to the freshness and thickness of the groundwater-bearing layer. The investigated area shows that the recharge originates from the south and not from the closest eastern adjacent bank of the reservoir due to the higher basement relief, the presence of compact sandstone, the direction of faults, and the presence of the hydrothermal solution. The above highlights that connectivity between these two water bodies is complex and does not abide by the geographical vicinity only but rather by the complexity of the structural elements in the area.

Furthermore, our findings reveal that the recharge to NSAS from HADR in the investigated area will continue as long as the reservoir level is above ~160 m. However, if the reservoir falls below this level, the reverse flow direction from the Nubian aquifer system to HADR can reduce the groundwater level in the adjacent areas to below ~160 m. The volume of this discharge is unquantified under monthly fluctuations in the HADR level. However, it can be a major factor under the prolonged drought or unilateral operation of upstream damming, where the reservoir can reach critical levels for multiple years. These unaddressed uncertainties could question the sustainable use of these groundwater resources around HADR. Proactive management and cooperation among Nile Basin countries is essential for addressing the above potential challenges and ensuring the sustainable management of both surface water and groundwater resources in the region.

Finally, to quantify the amount of reverse discharge from NSAS to HADR during its low-level operation period, which is beyond this preliminary investigation, current capabilities and data availability, accurate groundwater modeling, validated with more large-scale airborne hydrogeophysical surveys (Heggy et al., 2024), will be needed. For instance, using numerical simulation tools such as MODFLOW (Langevin et al., 2017) to model groundwater flow can constrain the uncertainties on the seepage volume from the High Aswan Dam to the Nubian Aquifer and vice versa. Such modeling would need several dataset entries, including the hydraulic conductivity, gradient, piezometric levels, and geologic cross-sections.

7. Consent to participate

The authors have read the final manuscript, given their approval for it to be submitted to the journal, and accepted full accountability for both the delivery of the manuscript and its content.

Ethical approval

This manuscript has not been published anywhere, nor is it currently being considered for publication anywhere.

CRediT authorship contribution statement

Mohamed Ramah: Writing – original draft, Visualization, Validation, Software, Methodology, Investigation, Data curation. **Essam Heggy:** Writing – review & editing, Visualization, Resources, Funding acquisition, Conceptualization. **Ahmed Nasr:** Resources, Project administration, Methodology, Formal analysis, Data curation, Conceptualization. **Mostafa Toni:** Writing – review & editing, Writing – original draft, Validation, Supervision, Conceptualization. **Mohamed M. Gomaa:** Writing – review & editing, Visualization, Supervision, Software, Project administration, Investigation, Formal analysis. **Emmanuel Hanert:** Writing – review & editing, Visualization, Validation, Supervision. **Adel Kotb:** Writing – review & editing, Supervision, Software, Project administration, Formal analysis, Conceptualization.

Declaration of competing interest

The authors declare that they have no known competing financial interests or personal relationships that could have appeared to influence the work reported in this paper.

Data availability

Data will be made available on request.

Acknowledgments

The authors thank Dr. Geoshy from the Desert Research Centre for his technical support in data collection during the fieldwork. The survey was funded by an award from Egypt's National Research Centre, Helwan University, and the Desert Research Center of Egypt . Part of this work is funded by the Zumberge Innovation Fund at the University of Southern California. Part of this research was carried out at the Jet Propulsion Laboratory, California Institute of Technology, under a contract with the National Aeronautics and Space Administration (NASA) (OASIS-USC-00630).

References

Abd Ellah, R.G., 2020. Water resources in Egypt and their challenges, Lake Nasser case study. Egypt. J. Aquat. Res. 46, 1–12.

Abd Ellah, R.G., 2021. Morphometric analysis of Toshka Lakes in Egypt: a succinct review of geographic information systems & remote sensing based techniques. Egypt. J. Aquat. Res. 47 (2), 215–221.

Abdelkhalek, A., King-Okumu, C., 2021. Groundwater exploitation in mega projects: Egypt's 1.5 million feddan Project. *Groundwater in Egypt's Deserts*, pp. 347-372.

Abdelmohsen, K., Sultan, M., Save, H., Abotalib, A.Z., Yan, E., 2020. What can the GRACE seasonal cycle tell us about lake-aquifer interac-tions? Earth Sci Rev 211, 103392.

Abotalib, A.Z., Abdelhady, A.A., Heggy, E., Salem, S.G., Ismail, E., Ali, A., Khalil, M.M., 2023. Irreversible and Large-Scale Heavy Metal Pollution Arising From Increased Damming and Untreated Water Reuse in the Nile Delta. Earth's Future 11 (3) e2022EF002987.

Abou Elmagd, K., Ali-Bik, M.W., Abayazeed, S.D., 2014. Geology and geochemistry of Kurkur bentonites, southern Egypt: provenance, depositional environment, and compositional implication of Paleocene-Eocene thermal maximum. Arab J. Geosci. 7 (3), 899–916.

Araffa, S.A.S., El-bohoty, M., Abou Heleika, M., Mekkawi, M., Ismail, E., Khalil, A.d., Abd EL-Razek, E.M., 2018. Implementation of magnetic and gravity methods to delineate the subsurface structural features of the basement complex in central Sinai area, Egypt. NRIAG J. Astron. Geophys. 162–174.

Awad, H., Kwiatek, G., 2005. Focal mechanism of earthquakes from June 1987 swarm in Aswan, Egypt, calculation by the moment tensor inversion. Acta Geophys. Polonica 53 (3), 275–291.

Azeem, M.A., Mekkawi, M., Gobashy, M., 2014. Subsurface structures using a new integrated geophysical analysis, South Aswan, Egypt. Arab. J. Geosci. 7 (12), 5141–5157.
Basheer, A.A., Ahmed, A., Kotb, A.D.M., 2024. Unveiling the Dynamics and Sustainability of the Nubian Aquifer System in El-Marashda, Egypt Through Geophysical, and Hydrogeochemical Investigations. Earth Syst. Environ. 1–18.
CONCO, 1987. Geological map of Egypt, NF 36 NW El Sad El Ali. Scale 1:500000. The Egyptian General Petroleum Corporation (GPC) and Conoco Co.
Basheer, A.A., Ahmed, A., Kotb, A.D.M., 2024. Unveiling the Dynamics and Sustainability of the Nubian Aquifer System in El-Marashda, Egypt Through Geophysical, and Hydrogeochemical Investigations. Earth Systems and Environment 1–18.
Diab, M.S., 1972. Hydrogeological and hydrochemical studies of the Nubian sandstone water bearing complex in some localities in United Arab Repuplic. Faculty of Sciences, Assuit University, p. 241. Ph. D. Thesis.
Ebraheem, M., Ramah, M., Omran, A., Sawires, R., Aal, G.A., 2016. 2D electrical resistivity imaging and seismic hazard assessment of building in Assiut New City, Egypt. In: 2016 SEG International Exposition and Annual Meeting. https://doi.org/10.1190/segam2016-13869515.1.
Egyptian Geological Survey and Mining Authority (EGSMA), 1981. Geological map of Egypt. Ministry of Industrial and Mineral Resources.
EI-Difrawy, M.F., 1988. Seismic and Geoelectric Studies of Subsurface Sediments at Shallow Depths, in the Area of Garf Hussein, South of Aswan, Egypt. Thesis, Cairo University, M.Sc.
Elba, E., Farghaly, D., Urban, B., 2014. Modeling high Aswan Dam reservoir morphology using remote sensing to reduce evaporation. Int. J. Geosci. 2014.
Eldardiry, H., Hossain, F., 2021. A blueprint for adapting high Aswan dam operation in Egypt to challenges of filling and operation of the Grand Ethiopian Renaissance dam. J. Hydrol. 598, 125708.
Elhaddad, H., Sultan, M., Yan, E., Abdelmohsen, K., Mohammad, A.T., Badawy, A., Karimi, H., Saleh, H., Emil, M.K., 2024. Optimization of floodwater redistribution from Lake Nasser could recharge Egypt's aquifers and mitigate its excessive floods. Commun. Earth Environ. 5 (1), 385.
El-Naggar, Z.R., 1970. On a proposed lithostratigraphic subdivision of the late Cretaceous- Early Paleogene succession in the Nile Valley, Egypt, U.A.R 7th Arab Petrol. Congr., Kuwait 1970, p. 64 (B-3), 1-50).
Elsawwaf, M., Feyen, J., Batelaan, O., Bakr, M., 2014. Groundwater–surface water interaction in lake Nasser, Southern Egypt. Hydrol. Process. 28 (3), 414–430.
Embabi, N.S., 2004. The geomorphology of Egypt, landforms and evolution, Volume I: The Nile Valley and the Western Desert. Spec. Pub., Egypt. Geograph. Soc. 447.
FAO, 2016. Egypt AQUASTAT-FAO's Information System on Water and Agriculture. Available online: http://www.fao.org/nr/water/aquastat/countries_regions/EGY/index.stm.
Fat-Helbary, R.E., Tealb, A.A., 2002. A study of seismicity and earthquake hazard at the proposed Kalabsha dam site, Aswan, Egypt. Nat. Hazards 25, 117–133.
Fathy, I., Ahmed, A., Abd-Elhamid, H.F., 2021. Integrated management of surface water and groundwater to mitigate flood risks and water scarcity in arid and semi-arid regions. J. Flood Risk Manage. 14 (3), e12720.
Fitterman, D.V., Stewart, M.T., 1986. Transient electromagnetic sounding for groundwater. Geophysics 51, 955–1005. https://doi.org/10.1190/1.1442158.
Fouad, S.S., Heggy, E., Abotalib, A.Z., Ramah, M., Jomaa, S., Weilacher, U., 2022. Landscape-based regeneration of the Nile Delta's waterways in support of water conservation and environmental protection. Ecol. Ind. 145, 109660.
Fouad, S.S., Heggy, E., Ramah, M., Abotalib, A.Z., Palmer, E.M., Jomaa, S., Weilacher, U., 2023. Egypt's waterways conservation campaigns under growing intrinsic demand and Nile upstream damming. J. Hydrol.: Reg. Stud. 50, 101537.
Gaber, A., Mohamed, A.K., El Galladi, A., Abdelkareem, M., Beshr, A.M., Koch, M., 2020. Mapping the groundwater potentiality of West Qena Area, Egypt, using integrated remote sensing and hydro-geophysical techniques. Remote Sens. (Basel) 12, 1559. https://www.mdpi.com/2072-4292/12/10/1559.
Geosoft Inc., 2010. Geosoft mapping and processing system. Geosoft Inc., Toronto, Canada.
Ghoubachi, S.Y., El-Abd, E.S.A., 2016. Hydrogeological studies for the Nubia sandstone aquifers in Garf Hussein area, Western Desert. Egypt. Arab. J. Geosci. 9, 596.
Gomaa, M.M., Zarif, F., Shenawy, A.E., Ramah, M., Kotb, A.D.M., 2024. Modelling and simulating the geoelectrical attributes of near-surface buried objects to optimizing its discovery. Modeling Earth Syst. Environ. 1–13.
Gonzales, A., Dahlin, T., Barmen, G., Rosberg, J.E., 2016. Electrical resistivity tomography and induced polarization for mapping the subsurface of alluvial fans: a case study in Punata (Bolivia). Geosciences 6, 51.
Hamdan, A.M., Selim, S.A., Abdallah, M.M., 2013. Interactions between the surface water and groundwater in the western shoreline of Lake Nasser, Upper Egypt. Arab. J. Geosci. 6, 77–84. https://doi.org/10.1007/s12517-011-0340-5.
Hanna, F., Osman, M.A.G., 1995. Agricultural land resources and the future of land reclamation and development in Egypt. Options Méditerranéennes, Sér. B, 9.
Hassan, A., Ismail, S.S., Elmoustafa, A., Khalaf, S., 2018. Evaluating evaporation rate from high Aswan Dam Reservoir using RS and GIS techniques. Egypt. J. Remote Sens. Space Sci. 21 (3), 285–293.
Heggy, E., Sharkawy, Z., Abotalib, A.Z., 2021. Egypt's water budget deficit and suggested mitigation policies for the Grand Ethiopian Renaissance Dam filling scenarios. Environ. Res. Lett. 16 (7), 074022.
Heggy, E., Ramah, M., Abotalib, A.Z., 2023. Examining the Accuracy of Using a Single Short-Term Historical Flow Period to Assess the Nile's Downstream Water Deficit from GERD Filling: A Technical Note. Earth Syst. Environ. 1–10.
Heggy, E., Moghaddam, M., Palmer, E.M., Brown, W.M., Blanton, J.L., Kosinski, M., Avouac, J.P., 2024. Airborne Sounding Radar for Desert Subsurface Exploration of Aquifers: Desert-SEA: Mission concept study [Space Agencies]. IEEE Geosci. Remote Sens. Mag. 12 (1), 162–185.
Heggy, E., Sharkawy, Z., Abotalib, A.Z., 2022a. Reply to Comment on 'Egypt's water budget deficit and suggested mitigation policies for the Grand Ethiopian Renaissance Dam filling scenarios' by Kevin Wheeler et al'. Environ. Res. Lett. 17 (12), 128001.
Heggy, E., Sharkawy, Z., Abotalib, A.Z., 2022b. Reply to Comment on 'Egypt's water budget deficit and suggested mitigation policies for the Grand Ethiopian Renaissance Dam filling scenarios. Environ. Res. Lett. 17, 088002.
Idriss, I., Arango, M., Savage, W., Youngs, R., Lee, K.W., 1985. Probabilistic Analysis of Potential Ground Motion Levels. InternalReport, High and Aswan Dams Authority, Egypt.
IPI2win (Version 3.0.1s). Moscow state university, 1990-2003 Version 2.6a (12.04.02).
Issawi, B., 1978. Geology of Nubia west area, Western Desert, Egypt. Ann. Geol. Surv. Egypt 8, 237–253.
Issawi, B., 1973. Nubian Sandstone: type section. Bull. A. A. P. G., pp.57:741-745.
Kim, J., Sultan, M., 2002. Assessment of the long-term hydrologic impacts of Lake Nasser and related irrigation projects in Southwestern Egypt. J. Hydrol. 262 (1–4), 68–83.
Kirsch, R. ed., 2006. Groundwater geophysics: a tool for hydrogeology. Berlin, Heidelberg: Springer Berlin Heidelberg.
Kivior, I., Boyd, D., 1998. Interpretation of the aeromagnetic experimental survey in the Eromanga/Cooper basin. Can. J. Explor. Geoph 34, 58e66.
Kotb, A., Basheer, A.A., Nasser, A., Ramah, M., 2021. Utilizing ERT and GPR to Distinguish Structures Maleficence the Constructions in the New Administrative Capital, Egypt. Earth 10 (5), 234–243.
Kotb, A.D.M., Hussein, G.H.G., ElHefnawy, M.A., 2014. Integrated geophysical study to explore the groundwater in the tectonic plain between Wadi El Mahash and Wadi Um Markhah, Southwest Sinai, Egypt. Arab. J. Geosci. 7, 2179–2197.
Kotb, A.D., Nabeh, M., Adham, A., 2021. Integrated remote sensing, VES, and TEM to evaluate the Rafah coastal aquifers for sustainable development—a case study. Arabian J. Geosci. 14 (17), 1697.
Langevin, C.D., Hughes, J.D., Banta, E.R., Provost, A.M., Niswonger, R.G., Panday, Sorab, 2017, MODFLOW 6 Modular Hydrologic Model: U.S. Geological Survey Software, https://doi.org/10.5066/F76Q1VQV.
McClymont, A.F., Roy, J.W., Hayashi, M., Bentley, L.R., Maurer, H., Langston, G., 2011. Investigating groundwater flow paths within proglacial moraine using multiple geophysical methods. J. Hydrol. 399 (1–2), 57–69.
Mekkawi, M., Grasso, J.R., Schnegg, P.A., 1982. Seismicity patternsat Lake Aswan, Egypt, 1982–2001. Bull. Seismol. Soc. Am. 94 (2), 479–492.
Mekkawi, M., Schnegg, P.A., Arafa-Hamed, T., Elathy, E., 2005. Electrical structure of the tectonically active Kalabsha fault, Aswan, Egypt. Earth Planet. Sci. Lett. 240, 764–773.
Metwaly, M.A., Khalil, M., Al-Sayed, E.S., Osman, S., 2006. A hydrogeophysical study to estimate water seepage from northwestern Lake Nasser, Egypt. J. Geophys. Eng. 3, 21–27.
Mosaad, S., Kotb, A.D., Basheer, A.A., 2024. Groundwater potentiality mapping: A case study in Baba and Sidri watersheds, South Sinai, Egypt. J. African Earth Sci. 210, 105145.
Nikiel, C.A., Eltahir, E.A., 2021. Past and future trends of Egypt's water consumption and its sources. Nat. Commun. 12 (1), 4508.
Rabe, T., Bedair, S., Miranda, M., Carvalho, J., Khalil, A., 2009. Subsurface Structures and Hydrogeologic Aquifers at the Western Side of Lake Nasser, Southwestern Desert, Egypt. J. Environ. Eng. Geophys. 14 (2), 87–95.
Ramah, M. (2021). Evaluation of the Nubian Sandstone Aquifer using Electrical Resistivity and Electromagnetic Methods at Northwest Nasser Lake Area, Aswan, Egypt. MSc thesis, Faculty of Science, Helwan University, Egypt.
Said, R., 1975. Some observations on the geomorphological evolution of the South Western of Egypt and its relation to the origin of the ground water. Ann Geol Surv Egypt 5, 67–70.
Selim, S.A. (1986). Inter relationship between the high dam reservoir and the groundwater in its vicinity- Ph.D. Thesis Aswan Fac.Sci., Assiut Univ., Egypt.
Shedid, M. (2006). Evaluation and management of groundwater resources in the area between Abu Simbel and Toshka, southwestern desert, Egypt. Ph.D. Thesis Fac. Sci., Minufiya Univ., Egypt.
Spector, A., Grant, F.S., (1970). Statistical models for interpreting aeromagnetic data. Geophysics 35, 293e302.
Sultan, S.A., Santos, F.M., 2009. Combining TEM/resistivity joint inversion and magnetic data for groundwater exploration: application to the northeastern part of Greater Cairo, Egypt. Environ. Geol. 58, 521–529.
Yousif, M. (2019). Hydrogeological inferences from remote sensing data and geoinformatic applications to assess the groundwater conditions. El-Kubbaniya basin, Western Desert, Egypt, Journal of African Earth Sciences 152.
Zondtem (version 5.2). (27.05.2016). Saint Petersburg University 2001-2016, http://zondgeo.ru/software/electromagnetic-soundings/.